Paper: ASAT-14-200-MO

14th International Conference on
AEROSPACE SCIENCES & AVIATION TECHNOLOGY,
ASAT - 14 – May 24 - 26, 2011, Email: asat@mtc.edu.eg
Military Technical College, Kobry Elkobbah, Cairo, Egypt
Tel: +(202) 24025292 –24036138, Fax: +(202) 22621908

Modeling and Performance Analysis of a Quad Detector

M.F. Heweage*, A.M. Mokhtar†, M.A. Soliman‡

Abstract: In this paper we are interested in modeling, performance evaluation, and measurement of a quadrant detector. Photodiode is modeled using its differential equations then implemented and solved using ORCAD -pspise. The model validation was performed by comparing the model results with the experimental measurements using a proposed setup. The model was used to investigate the effect of the photodiode donor concentrations, acceptor concentrations and intrinsic region concentrations. The simulation results showed that the donor concentrations should be kept as small as possible in order to improve the photodiode performance, the acceptor concentrations has a small effect on the performance, and as the intrinsic region concentration increases the photocurrent increases and the junction capacitance decreases with a small increase in the dark current.

Keywords: Photodiode modeling, Quad detector, photodiode performance measures

1. Introduction

A photo sensitive detector (PSD) is a continuous silicon photo detector used for optical position sensing and basically consists of a uniform resistive layer, which is formed on a silicon substrate. A pair of electrodes is formed at the ends of the resistive layer from which photo-currents are measured. These photo-currents are generated as a result of the incident radiation effect as shown in figure (1) and their magnitude is relative to the distance of the electrode to the center of the beam spot on the sensor's active area. The photo-currents are typically amplified and converted to form the measured voltage signal used by the control system. PSDs can be divided into two general groups: segmented PSDs and lateral effect PSDs [1].

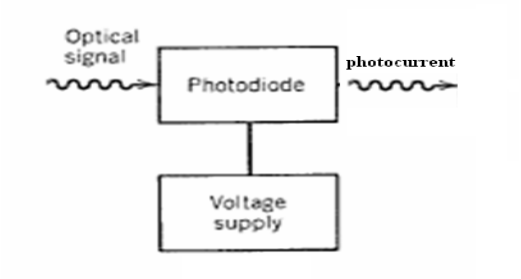

Fig. 1 Photodiode transfer function

As shown in figure (2) Segmented PSD are quadrature PSD each is divided into four segments, which are separated by a small gap, called the dead region. The sensor is used for positioning by measuring each segment's photocurrent. A symmetrical beam is positioned at the center of the QD if all of these currents are equal [2].

* Egyptian Armed Forces, fte7a_82@hotmail.com
† Egyptian Armed Forces, ayman_mokhtar@hotmail.com
‡ Egyptian Armed Forces

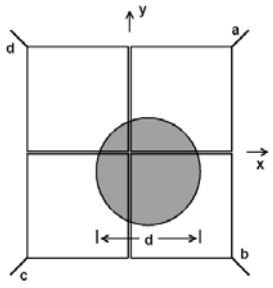

Fig. 2 Quadrant detector structure

Figure (3) shows the equivalent circuit diagram for the photodiode where I_P is the photo generated current, I_d is the dark current, I_N is the internal noise current, R_{SH} is the shunt resistance, R_S is the series resistance, C_J is the junction capacitance and the output photocurrent is taken at the load of the detector [3 , 4].

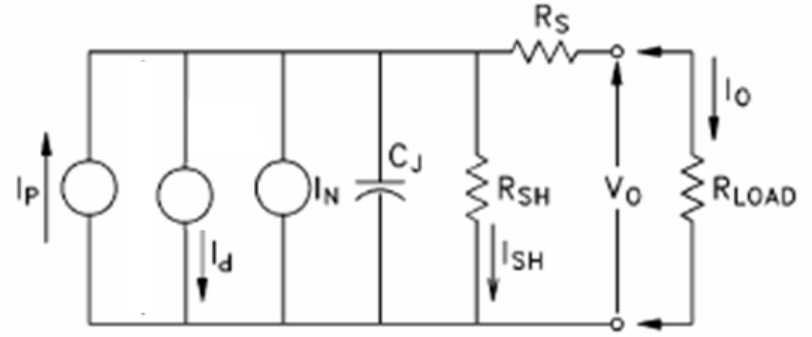

Fig. 3 Equivalent Circuit diagram for the photodiode

2. Photodiode Modeling

In this paper we will present the model of a single photodiode which is considered as the building unit of the quad detector. Starting with the differential equation (1) the depletion region of a pin photodiode in reverse bias supports a constant electric field and linearly varying energy bands. From Poisson's equation we have [5]

$$\frac{d^2\Phi}{dx^2} = \frac{q}{\varepsilon}\left(N_d^+ + N_A^- + p - N\right) \approx 0 \tag{1}$$

where q is the electron charge, ε is the electric field, $\acute{A}$ is a linear function of position, N^+_d is the ionized donor concentration impurities, N^-_A is the acceptor concentration impurities, the density of electron in the conduction band is n and that of holes in the valance band is p.

If we neglect the intrinsic region background doping and assume that the generated photo charge is negligible or quasi-neutral this implies that Φ is a linear function of position. The main contribution of the photocurrent is given by the drift current associated with carriers generated inside the intrinsic depleted region;

$$G_0(x) = \eta Q \frac{P_{in}(1-R)}{Ahf}\alpha e^{-\alpha x} = G_0(0)e^{-\alpha x} \tag{2}$$

where $G_o(x)$ is the optical generation rate along X-axis, ηQ is the intrinsic quantum efficiency, P_{in} is the total incident power on the left (upper) photodiode facet, A is the detector area, hf is the photon energy, α is the material absorption, and R is the power reflectivity of the upper surface.

To analyze the DC pin current I_{PD} we decompose the total current into electron current (drift and diffusion) and hole current (drift and diffusion) components. The device current is constant in x and can be expressed as [5, 6]. The absorption coefficient of the material (α) can be calculated from [7].

$$\log\alpha = (13.2131 - 36.7985\lambda + 48.1893\lambda^2 - 22.7562\lambda^3) \tag{3}$$

The total photodiode current is given by:

$$-I_{PD} = \frac{qAD_{np}}{W_p} n_0' + \frac{qAD_{hn}}{L_{hn}} p_0' - \left[\frac{qAG_0(0)L_{hn}}{1+\alpha L_{hn}} e^{-\alpha(W+W_p)} + I_i \right] \tag{4}$$

where the first term is the dark current and the second term is the photocurrent. Expanding the generation rate *Go* and using equation (2) the photocurrent can be expressed as [5, 6]

$$I_L = \eta Q \frac{q}{hf} P_{in}(1-R)e^{-\alpha W_p}\left(1 - \frac{e^{-\alpha W}}{1+\alpha L_{hn}}\right) \tag{5}$$

(Equation (5) holds when α Wp is small, since photocurrent generation in the top layer is explicitly neglected.) thus leading to the responsivity.
According to the general equation studied before we used the orcad pspice tool to model the photodiode and simulate the output [8 , 9], then compare the output with the datasheet or measured data. From the equivalent circuit model of the photodiode and according to the equation that represents each part in the circuit model we built the model, where each block of the model represents a set of equations which provide the simulation of the photodiode behavior, figure (4) shows ORCAD photodiode model. Every part of this equation must be in general form, so that it is possible to change its parameters. The challenge was how to solve this with the orcad tool and the analog behavior model (ABM) was the suitable solution. With the help of the electronic part to achieve the photodiode behavior, the ABM helped us to use and represent the equation for each part of the model with the accepted behavior and function. The parameters which forms the equation must be given to built the photodiode model and provide the accepted data with the real photodiode.

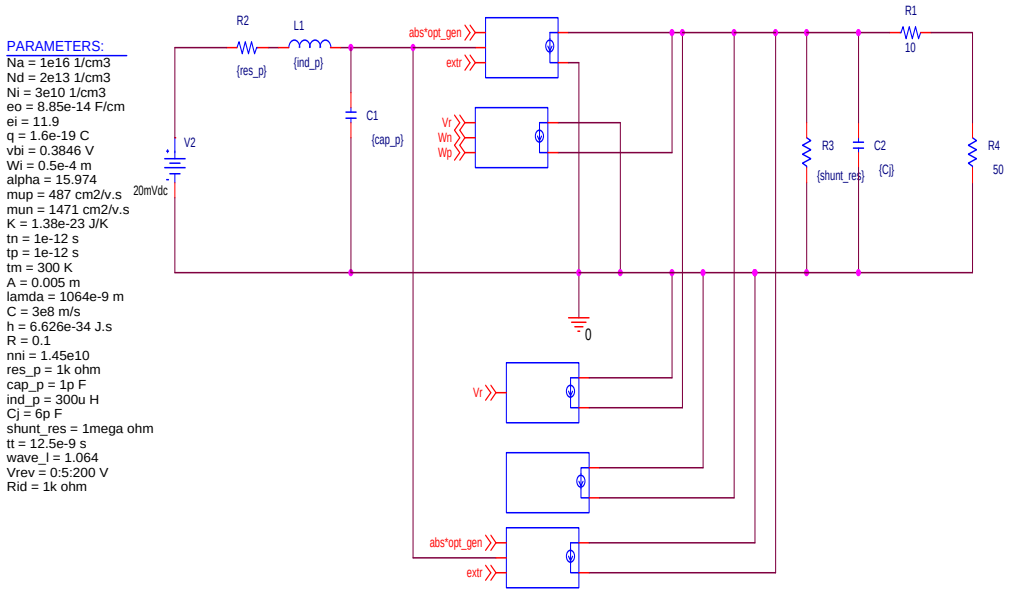

Fig. 4 ORCAD Photodiode model

3. Photodiode Model Validation

This paper discusses the method and tools that are used to measure the photodiode parameters. There are three parameters that can be measured by the proposed setup: photocurrent, dark current, and junction capacitance. Figure (5) shows the proposed setups that are used to measure the above parameters. The setup consist of Г5-88 pulse generator , GOS-6031 oscillograph , LFR Sensitivity , GDM- digital voltmeter , GPR3HIDD power supply and, laser source its wavelength is 1.064 *um*

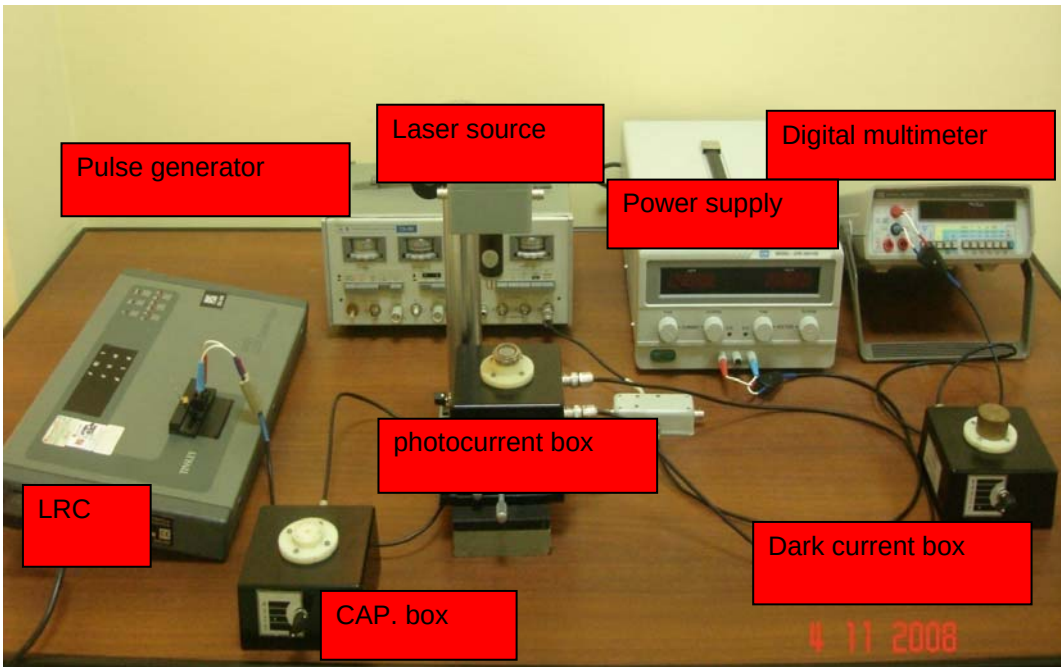

Fig. 5 Photodiode parameter measurement setup

Figure (6) shows the proposed setup that is used to measure the photocurrent output from the photodiode due to the incident radiation beam on the photodiode surface area.

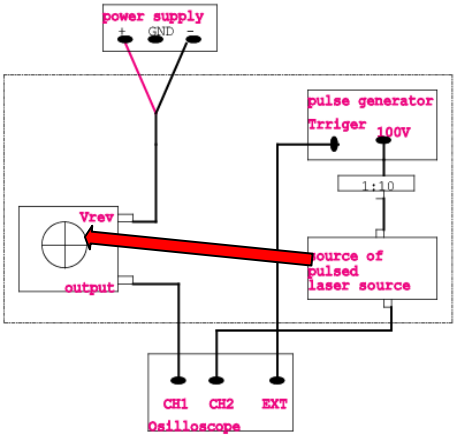

Fig. 6 Photocurrent measurement setup

Figure (7) shows the proposed setup that is used to measure the dark current output from the photodiode in the absence of incident radiation. Figure (8) shows the proposed setup that is used to measure the junction capacitance of the photodiode in the absence of incident radiation.

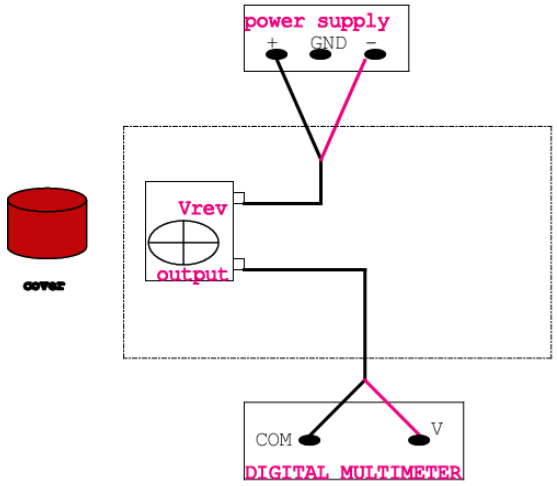

Fig. 7 Dark current measurement setup

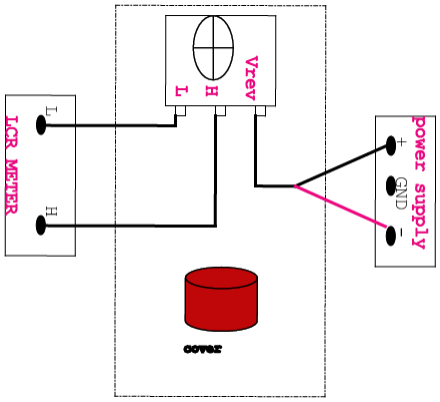

Fig. 8 Junction capacitance measurement setup

4. Simulation Results and Analysis

Figures 9 and 10 show the simulated and measured output pulse at the load of the photodiode when the input pulse incident on the photodiode is the same for both measured and simulated cases. The simulated output signal has a good agreement with the measured pulse where the amplitude has the same value (around 100mV*)*, the pulse width also has the same value (5 *usec*), and the period time is the same (50 *usec*). The measured fall time of the pulse is the same in the two pulses (fall time=0.28 *usec*), Fig. 9.

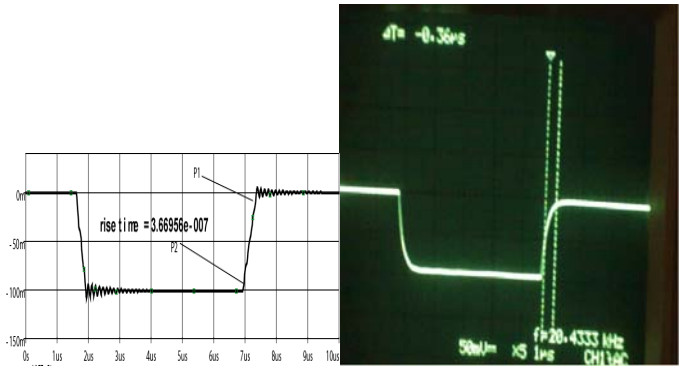

Fig. 9 Simulated and measured pulse rise time

Likewise, the measured rise time of the pulse is the same in the two pulses (rise time= 0.36 *usec*), Fig. 10.

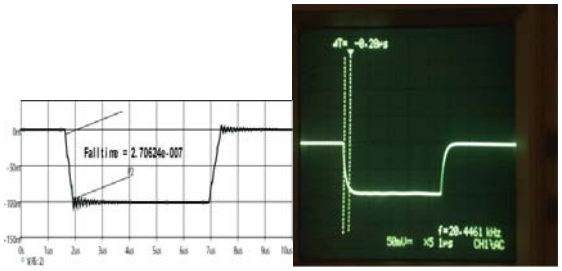

Fig. 10 Simulated and measured pulse rise time

Figure 11 shows the relation between the junction capacitance and the reverse bias volt for both measured and simulated values; we can see the good agreements between the four measured values and the simulation values.

It is clear that the junction capacitance decreases as the reverse bias volt increases until it reaches value of the reverse bias near saturation value in which the decrease of the junction capacitance is very small.

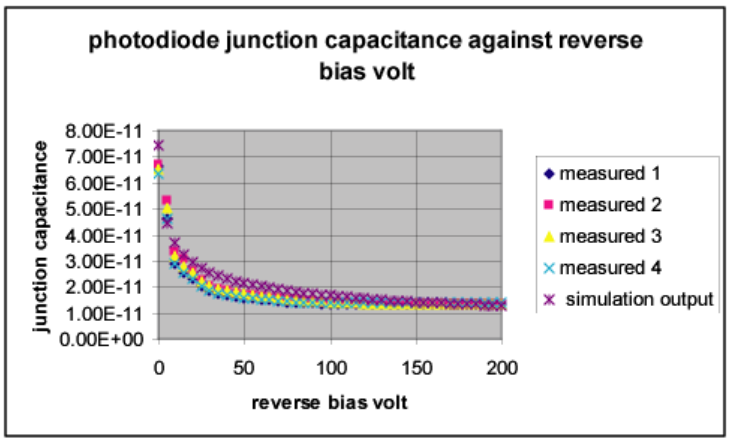

Fig. 11 Simulated and measured values of a junction capacitance

Figure 12 shows the relation between the dark current and the reverse bias volt for both measured and simulated values, we can see that there is a good agreement between the four measured and the simulated valued.

It is clear that the dark current increases as the reverse bias volt increases, we can conclude that from the photodiode measured and simulated results shown in the previous pages.

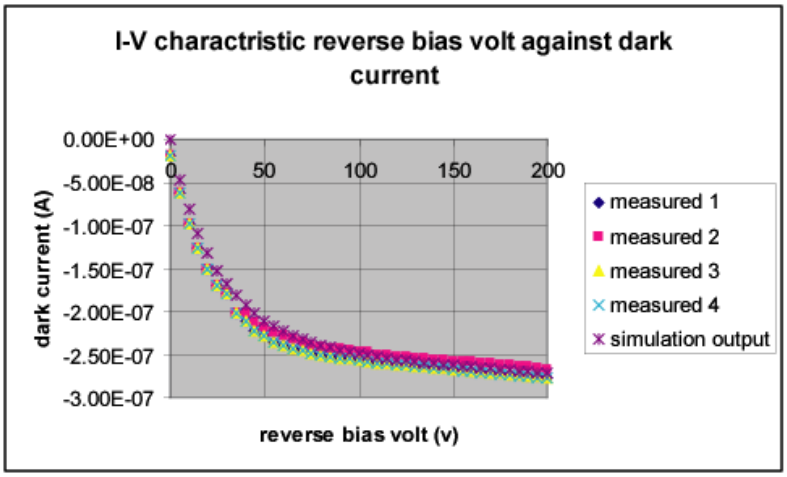

Fig. 12 Simulated and measured values of dark current

From figures 9, 10, 11, and 12 it is clear that we must apply a reverse bias to the photodiode to decrease the capacitance and increase the photocurrent which will increase the photodiode sensitivity with the small increase on the dark current.

The effect of the photodiode material parameters on the photodiode performance will be discussed in the remainder of this paper.

The photodiode material has a great effect on the performance of the detector we will discuss this parameter and its effect in terms of donor concentration, acceptor concentration and intrinsic region concentration.

We will show the effect of each parameter on the junction capacitance, dark current and photocurrent.

Figure 13 shows the effect of the donor concentration on the photodiode junction capacitance, Nd was swept from N_d=1e13 to N_d=1e14 with the step N_d=1e13. It is clear that the junction capacitance value shifted to higher values with the increase of the N_d .

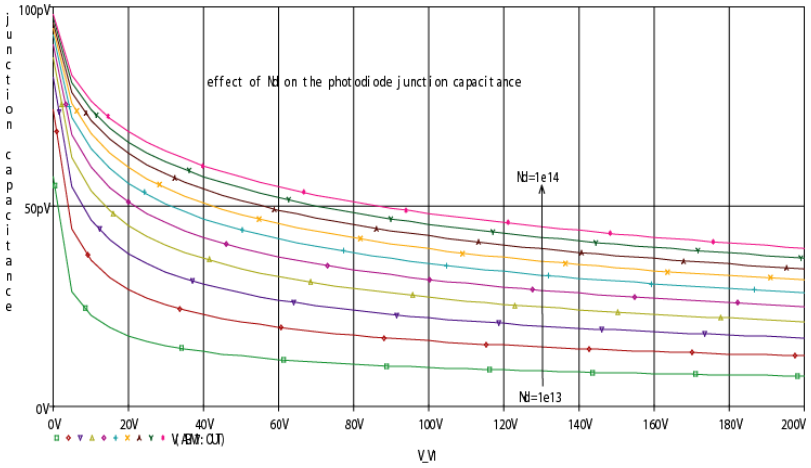

Fig. 13 Junction capacitance vs. reverse volt for different donor concentration

Figure 14 shows the effect of the donor concentration on the photodiode dark current, N_d was swept from N_d =1e13 to N_d =1e14 with the step N_d =1e13. It is clear that the dark current value shifted to lower values with the increase of the N_d.

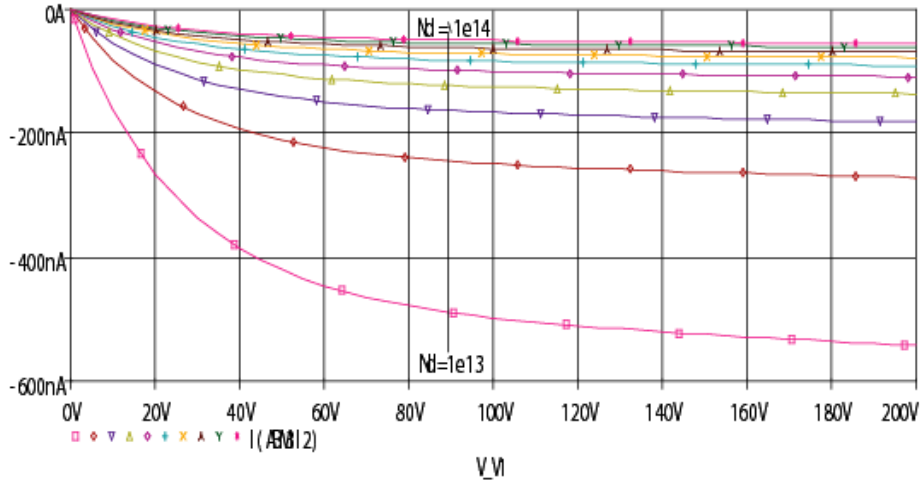

Fig. 14 Dark current vs. reverse volt for different donor concentration

Figure 15 shows the effect of the donor concentration on the photodiode output photocurrent pulse, N_d was swept from N_d =1e13 to N_d =1e14 with the step N_d =1e13. It is clear that the photocurrent value shifted to lower values with the increase of the N_d.

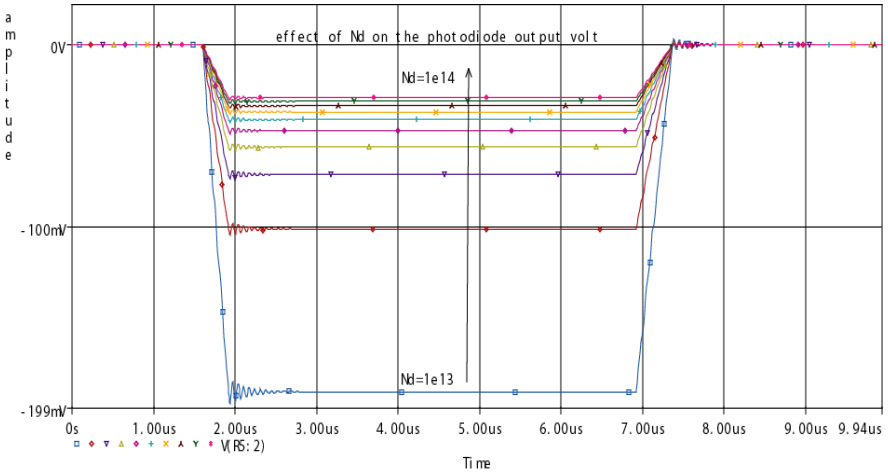

Fig. 15 Output pulse vs. time for different donor concentration

We can conclude the effect of the donor concentration on the photodiode from figures 13, 14, and 15 that as the donor concentration increases the value of the junction capacitance increases, and both of the dark current and photocurrent decreases.

To improve the photodiode performance we must decrease the junction capacitance and dark current with the increase of the photocurrent, so we have to choose the donor concentration as small as possible.

Figure 16 shows the effect of the acceptor concentration on the photodiode junction capacitance, Na was swept from N_a=1e16 to N_a =1e17 with the step N_a =1e16. It is clear that from the figure the junction capacitance value appeasers to be constant.

Figure 17 shows the effect of the acceptor concentration on the photodiode dark current, Na was swept from N_a =1e15 to N_a =1e16 with the step N_a =1e15. It is clear that the dark current slightly decreases with the increase of N_a.

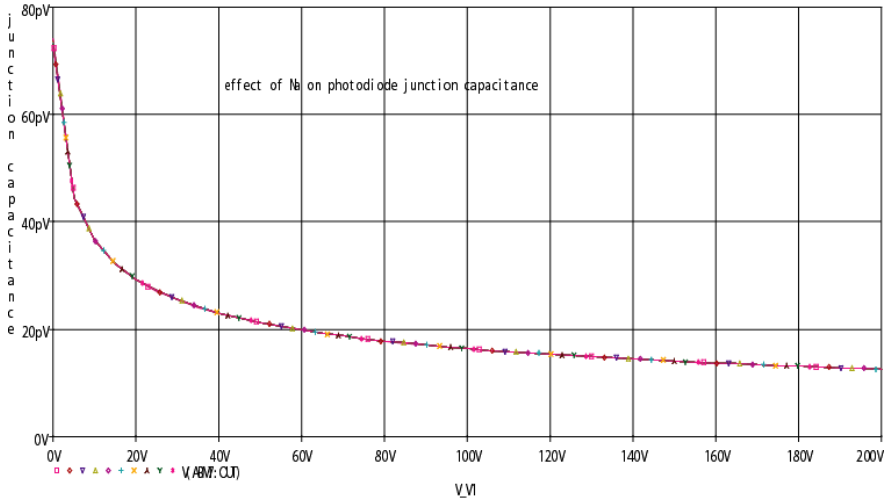

Fig. 16 Junction capacitance vs. reverse volt for different acceptor concentration

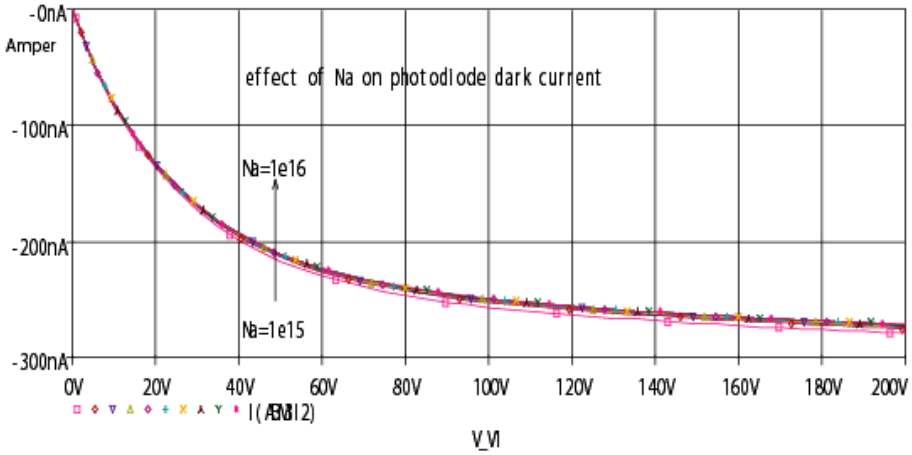

Fig. 17 Dark current vs. reverse volt for different acceptor concentration

Figure 18 shows the effect of the acceptor concentration on the photodiode output photocurrent pulse, N_a was swept from N_a =1e15 to N_a =1e16 with the step N_a =1e15. It is clear that the photocurrent slightly decreases with the increase of N_a.

We conclude the effect of the acceptor concentration on the photodiode from Figures 16, 17, and 18 that with the increase of the acceptor concentration the value of the junction capacitance remains nearly the same, the dark current decreases slightly, and photocurrent remains nearly the same, so that we must chose the value of the acceptor concentration with the smallest dark current value.

Figure 19 shows the effect of the intrinsic region concentration on the photodiode junction capacitance, Ni was swept from N_i=1e10 to N_i =1e11 with the step N_i =1e10. It is clear that the junction capacitance decreases with the increase of N_i .

Figure 20 shows the effect of the intrinsic region concentration on the photodiode dark current, Ni was swept from N_i =1e10 to N_i =1e11 with the step N_i =1e10. It is clear that the dark current increases with the increase of N_i.

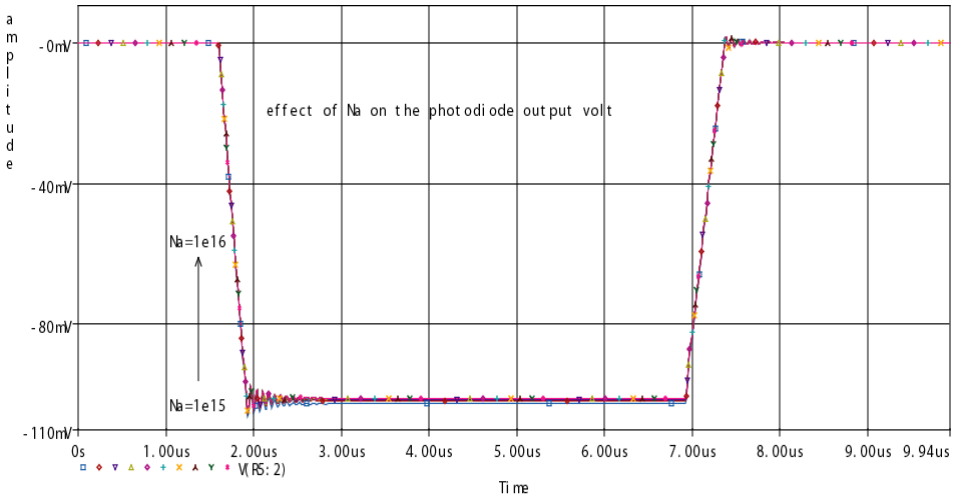

Fig. 18 Output pulse vs. time for different acceptor concentration

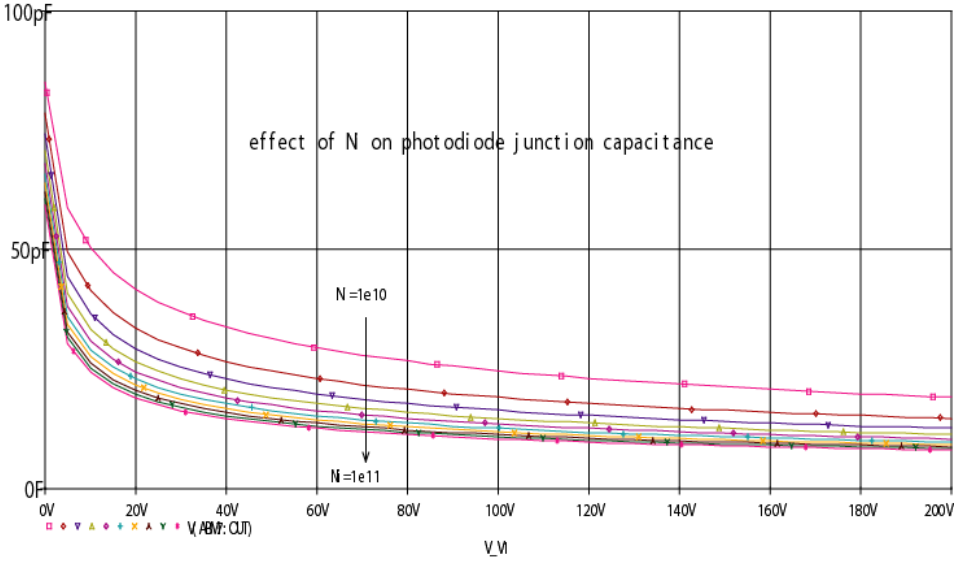

Fig. 19 Junction capacitance vs. reverse volt for different intrinsic region concentration

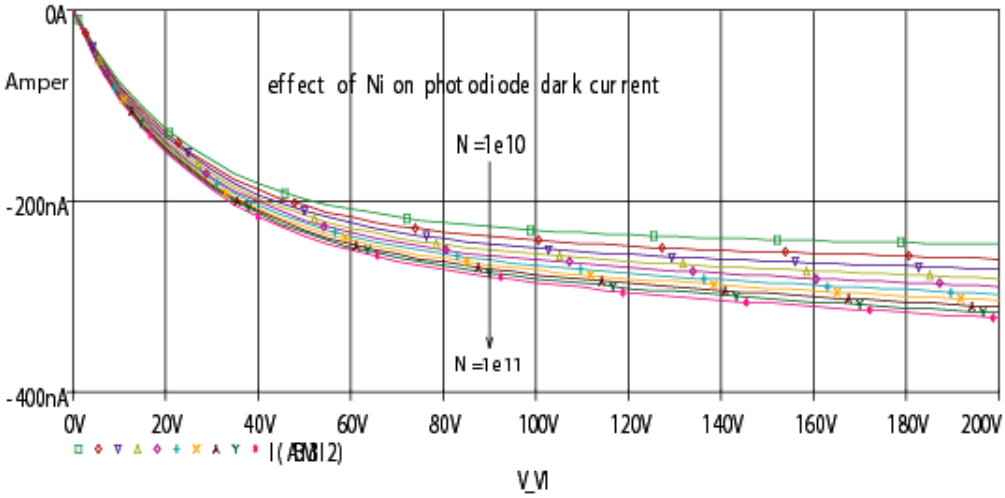

Fig. 20 Dark current vs. reverse volt for different intrinsic region concentration

Figure 21 shows the effect of the intrinsic region concentration on the photodiode output photocurrent pulse, N_i was swept from N_i =1e10 to N_i =1e11 with the step N_i =1e10.
It is clear that the photocurrent increases with the increase of N_i.

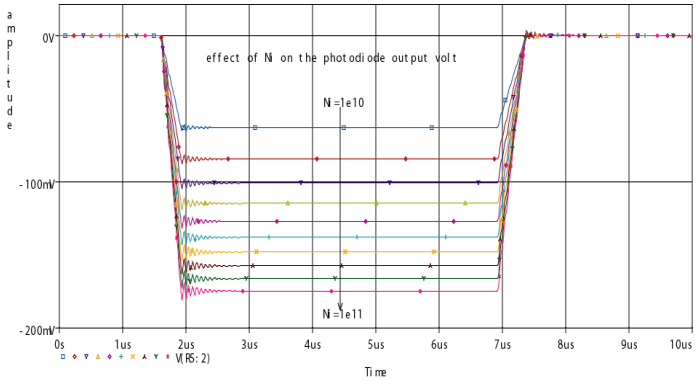

Fig. 21 Output pulse vs. time for different intrinsic region concentration

We can conclude the effect of the intrinsic region concentration on the photodiode from figures 19, 20, and 21 that with increasing of the intrinsic region concentration the value of the junction capacitance decreases and the photocurrent increases but the dark current slightly increases. To improve the photodiode performance we must increase the photocurrent with the decrease of the dark current and the junction capacitance so that we have to choose the largest possible value for the intrinsic region concentration.

5. Conclusion

Photodiode model was implemented in ORCAD pspise tool, the validation of the model using a proposed setup was performed, a good agreement was achieved between the measured and simulated results. The model was used to analyze the performance of the photo diode where the effect of the different parameters of the photodiode material on its performance were investigated.

6. References

[1] G. Knoll, Radiation Detection and Measurement, 3rd ed. Wiley, 1999.
[2] D. Decoster and J. Harari, Optoelectronic Sensors. online ISTE Ltd., 2009.
[3] S. Donati, Photodetectors: Devices, Circuits, and Applications. Prentice Hall, 2000.
[4] K. BRENNAN, Introduction to Semiconductor Devices. cambridge university press, 2005.
[5] G. Ghione, Semiconductor Devices for High-Speed Optoelectronics, ser. 1 st. The Edinburgh Building, Cambridge CB2 8RU, UK: PRESS cambridge university press, 2009, vol. 4.
[6] S. S. Li, Semiconductor Physical Electronics, 2nd ed. Springer Science+Business Media, LLC, 2006.
[7] H. Melchior, \Demodulation and photodetection techniques," Laser Handbook F. T. Arecchi and E.O. Schulz-Dubios, vol. 1, pp. 725{835, 1972.
[8] R. J. Perry and K. Arora, \Using pspice to simulate the photoresponse of ideal cmos integrated circuit photodiodes," IEEE, 1996.
[9] L. Castaner and S. Silvestre, Modelling Photovoltaic Systems using PSpice. John Wiley and Sons Ltd, 2002.